Energy and Buildings 139 (2017) 101–107

Contents lists available at ScienceDirect

Energy and Buildings

journal homepage: www.elsevier.com/locate/enbuild

Estimating solar energy potentials on pitched roofs

Yan Li, Chunlu Liu *

School of Architecture and Built Environment, Deakin University, Geelong, Australia

ARTICLE INFO

Article history:
Received 11 August 2016
Received in revised form 9 November 2016
Accepted 24 December 2016
Available online 6 January 2017

Keywords:
Building roofs
Building simulation
Modelling
Programming
Solar energy assessment

ABSTRACT

Pitched-roof buildings make up a considerable proportion of architectural roof styles. Precise estimation of solar energy potential on pitched roofs is thus crucial to the sustainable development and renewable energy consumption of human habitats. Conventional solar radiation measurements usually adopt Light Detection and Ranging (LiDAR) data, which can only be extracted from existing buildings. There has been relatively little research assessing solar radiation on pitched roofs. This paper develops a pixel-based approach to estimation of solar energy potentials over pitched roofs based on the pretext of architectural design drawings. A typical Australian house with nine roofs is then chosen for implementation through a case study. The solar radiation on a certain cell of a shadow map is mathematically formulated for each pixel unit. Its yields over a certain time period are calculated by considering multiple instantaneous solar irradiances and visually presented through image processing. The resulting solar radiation maps, especially a coloured 3D map, reveal the roofs' radiation distribution including effects from objects on the roofs such as chimneys. Radiation contour lines are mapped to obtain installation ranges for solar devices. This study will benefit commercial energy investors, residents and urban planners in the efficient use of renewable energy sources through accurate prediction of solar radiation potential and identification of areas receiving high radiation over sloping roofs.

1. Introduction

Renewable energy can be considered an ideal solution to energy challenges, such as the depletion of fossil fuel reserves and environmental pollution [1]. Solar energy dwarfs other renewable and fossil-based energy resources, since it is recognised as a clean, free, unlimited, easily accessible, and environmentally and economically friendly energy source [2]. In urban areas, exterior building surfaces, especially roofs, are commonly considered suitable places to install solar collectors for producing usable energy. These devices require little maintenance and offer high returns on investment, and can achieve energy conversion without noise or greenhouse gases.

The direct utilisation of solar energy in buildings mainly occurs via solar photovoltaic technologies, which aim to absorb solar radiation and generate electricity directly using photovoltaic cells, and thermal technologies, which are used to preheat domestic hot water and/or to cover a fraction of the space heating demand [3]. Furthermore, the utilisation of solar energy sources is cost effective. Compared to conventional energies, an investment in solar equipment provides long-lasting energy for current and future generations. Use of solar energy can also contribute to green building rating systems [4]. Thus, solar energy presents an ideal solution in energy consumption of buildings and environmental health of modern sustainable cities. Previous technology research has made great efforts in the search for low-cost manufacturing of solar devices [5]. The solar radiation potential is much reliable for identifying the most suitable roof surfaces of installing solar collectors [6]. It is, therefore, necessary to evaluate solar energy potential and analyse its distribution over building roofs in order to promote efficient use of solar energy and satisfy as much urban energy demand as possible. In addition, pitched roofs are a commonly used architectural style. Yet evaluation of solar energy potential for urban use is a challenge, since there are significant spatial and temporal variations in solar radiation that are greatly affected by various factors such as surface orientation and shadowing effects [7].

To estimate solar radiation potential over given building surfaces, researchers have explored and developed several models and technologies [8]. Light Detection and Ranging (LiDAR) mapping is a widely used method of measuring solar energy potential [9]. Since data about height grids in urban environments is easily accessible through airborne LiDAR surveys, use of remote sensing data has become popular in solar energy estimation on extracted building

* Corresponding author at: School of Architecture and Built Environment Waterfront Campus, Deakin University, 1 Gheringhap Street, Geelong, Victoria 3220, Australia.
E-mail address: chunlu@deakin.edu.au (C. Liu).

http://dx.doi.org/10.1016/j.enbuild.2016.12.070
0378-7788/

footprints. LiDAR-based data acquisition technology allows for the rapid reconstruction of terrain surfaces when assessing building insolation with existing 2D models [10].

In 2009, LiDAR data was employed by Tereci et al. [11] to build a Digital Surface Model (DSM). The annual solar potential was then determined for identified building roofs in combination with ALK map data and GIS software. On the basis of the use of LiDAR and 2D/3D vector data, a 2.5D DSM was constructed by Lee and Zlatanova [12] for computing the morphological properties of buildings. This tool for solar radiation calculation is not only suited to roofs but also useful for analysis of building facades. In 2013, in order to estimate solar potential over building surfaces, Redweik et al. [13] also proposed a solar radiation method based on the *r.sun* radiation model developed by Šúri et al. [14] and incorporated this in the open source GRASS GIS [15]. Their results revealed that the solar potential of building facades is lower than that of roofs, although facades normally have larger areas. Taking advantage of ESRI's Solar Analyst Toolbox and LiDAR data, Kodysh et al. [16] introduced a method for estimating solar potential on multiple building rooftops through combining a DEM with an upward-looking hemispherical viewshed algorithm. Lukač and Žalik [17] presented a method using graphics processing units with computed unified device architecture technology and LiDAR data for solar potential estimation. In addition, some evolutionary approaches have been applied in the optimal design of solar building models based on LiDAR data [8,18]. However, LiDAR-based procedures often have a high computational cost due to the need for data detection by aircraft and are more suited to existing buildings. Energy investors may be restricted by data availability and measurements may be limited to simple roofing structures.

Constructing 3D models has been applied to solar radiation estimation. In 2011, Hachem et al. [19] chose two-storey single housing units as case studies to investigate the effects of roof shape on solar energy potential. Thereafter, researchers have considered that 3D visualisation facilitates the assessment of photovoltaic potential on building surfaces and suits more building types [20]. Inspired by a combined vector–voxel solar radiation model, Liang et al. [21] computed solar potential building models through a method in which 3D vector objects were all segmented into polygonal elements using a voxel-intersecting rule and 3D meshes were discretised into a set of 2D raster cells. However, rapid development and wide use of solar energies in urban areas necessitate more accurate measurement of solar resources, which means that higher resolution photography is essential in order to demonstrate the spatial–temporal distribution of solar potential over building surfaces and provide accurate statistical analysis. In addition, previously constructed models oversimplify the complex topographic features of building roofs, so that the resulting maps cannot identify effects from objects erected on roofs.

Recently, a pixel-based approach was presented by Li et al. [22] for estimating solar energy potential on flat roofs. This paper develops a pixel-based method for pitched roofs by determining the solar radiation through an application programming interface constructed in the SketchUp platform. Based on digital image processing using MATLAB, this method allows for the estimation of solar potential yields on sloped rooftops through formulating solar irradiances in pixel units. Solar radiation yields over a certain time period with minute-level accuracy are then calculated by considering multiple instantaneous solar irradiances and visually presented through image processing. In this paper, a typical Australian house with nine roofs is chosen for implementation through a case study. Statistical analysis and potential distribution with centimetre-level accuracy enhance assessment measures. Radiation contour lines are then mapped for outlining installation ranges of solar devices over roof surfaces. The proposed method is detailed in the next section.

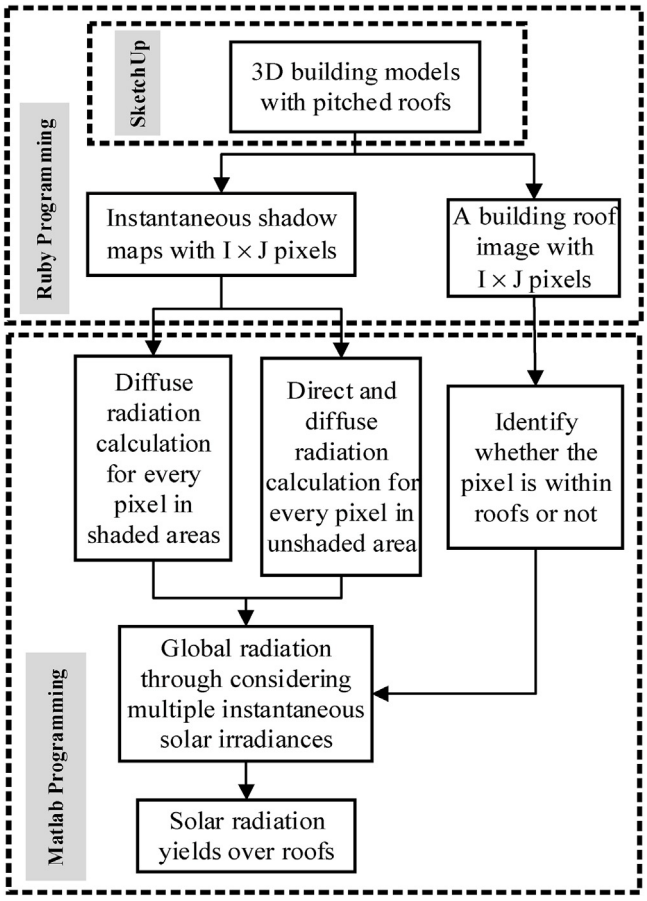

Fig. 1. A flowchart to calculate solar radiation yields over a pitched roof.

2. A framework for estimating solar radiation on pitched-roof buildings

The LiDAR-based procedure starts with data collection through aerial detection and constructs a continuous DSM in which the raster size usually ranges from 0.3 m to 1 m [6,13,23]. Unlike previous methods, the pixel-based procedure begins with building models based on existing or planned buildings. In the Ruby programming environment provided in the SketchUp platform, a series of high-resolution shadow maps are produced so that the measurement can preserve the topographic features of the building surfaces. Based on digital image processing with MATLAB, the data from each pixel can be independently processed within the uniform square grid data structure. The whole workflow of the pixel-based method is illustrated in Fig. 1 taking a simple pitched-roof building as an example.

Firstly, 3D building models are constructed through the modelling platform SketchUp. When considering a complex built environment, terrain data can also be taken into account in the form of elevation contour lines to describe the continuously varying topographic surfaces. To produce a complex shadowing situation, various surrounding objects, such as structures, infrastructure and plants, can also be modelled. Their shadows can then be casted with solar conditions in SketchUp.

Secondly, shadowing effects at any time can be illustrated by an image in which the whole domain is equally discretised by pixels. As shown in Fig. 2, the upper picture demonstrates a 3D shading model for a single pitched-roof building. The lower picture depicts

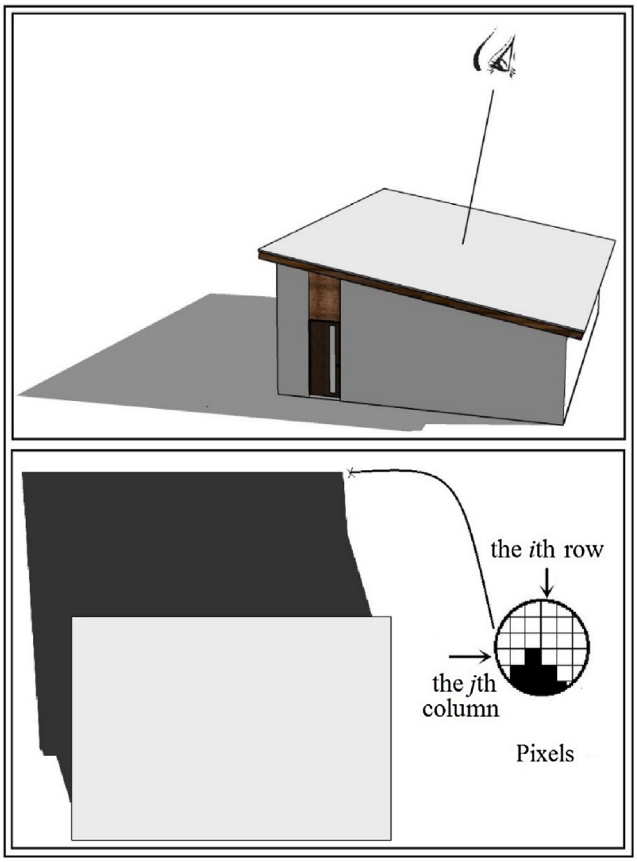

Fig. 2. A single pitched-roof model and its shadow map.

a shadow map of the building from a top view, but the line of sight is perpendicular to the roof surface, as in the upper picture. For a shadow map at a time point, the pixel value of the greyscale image V_{pixel} is a single number that represents the brightness of the pixel. The most common pixel format is the byte image, in which this number is stored as an 8-bit integer that ranges from 0 to 255. Black and white pixels are therefore used to indicate shaded and unshaded cells respectively in an instantaneous shadow map. Based on the Ruby console in SketchUp, a series of instantaneous shadow maps are produced after casting visible shadows with the building models. All the shadow maps have the same image dimensions and are from the same view. A binary image of the rooftop is also produced by SketchUp from the same view. Pixels that represent roofs are displayed as black and the rest are referred to as the background colour, white.

Thirdly, the algorithm implements radiation estimation calculation for pixels. In this paper, the basic algorithm of solar radiation estimation is implemented in terms of the approach presented by Kumar, et al. [24]. Specifically, solar declination δ and hour angle h can be obtained to identify the Sun's position in the sky. That is to say, based on the latitude of a site L, the altitude angle α can be defined as:

$$\sin\alpha = \sin\ L \cdot \sin\ \delta + \cos\ L \cdot \cos\ \delta \cdot \cos\ h \tag{1}$$

The optical air mass M can then be written as:

$$M = \left[1229 + (614\ \sin\alpha)^2\right]^{0.5} - 614\ \sin\alpha \tag{2}$$

Solar flux I_o (W/m^2), atmospheric transmission of direct radiation τ_b and diffuse radiation τ_d can be expressed as Eqs. (3)–(5).

$$I_o = S_o\left[1 + 0.0344\cos\left(360^\circ N/365\right)\right] \tag{3}$$

$$\tau_b = 0.56\left(e^{-0.65M} + e^{-0.095M}\right) \tag{4}$$

$$\tau_d = 0.271 - 0.294 \times \tau_b \tag{5}$$

in which N is the number of days since 1st January and the solar constant S_o is set as 1367 W/m^2 [25].

Direct solar radiation I_b can be formulated as Eq. (6) when the Sun's rays are striking a surface whose normal pitch makes an angle θ with the direction to the Sun. θ relies mainly on spatial factors, such as the slope and aspect of the surface, and temporal factors, such as the solar azimuth and altitude. η denotes the location-based sunshine percentage and aims to consider the probability of a cloudy sky. Diffuse solar radiation I_d can be formulated as Eq. (7) for a building with a roof pitch angle β.

$$I_b = \eta \times I_o \times \tau_b \times \cos\ \theta \tag{6}$$

$$I_d = I_o \times \tau_d \times \cos^2\beta/2\ \sin\ \alpha \tag{7}$$

When solar radiation strikes a particular site, the total radiation is equal to the sum of the direct and diffuse solar irradiances for an unshaded site. On the other hand, the total radiation excludes direct solar radiation if the site is in shadow. This is because, unlike diffuse radiation, direct radiation cannot reach a shaded site.

Accordingly, the pixels can all be identified as either shaded or unshaded through MATLAB programming, which reads each pixel value in the shadow maps. Diffuse radiation calculation is implemented if a pixel is identified as shaded. Otherwise the program calculates the direct and diffuse radiation. In this research, a pixel of value between 0 and 250 is taken to be a shaded cell on a shadow map, where 250 is selected as the threshold value. A pixel of value from 250 to 255 is considered an unshaded cell. The area for each cell A_{cell} is used to indicate the actual area on a map that the pixel represents in an image. Therefore, the Nth daily solar radiation yield for the pixel cell located in the ith row and jth column $E^N_{cell_{i,j}}$ can be obtained by integrating the instantaneous solar irradiances within the time interval [*sunrise*, *sunset*]. Based on the actual cell area, daily global irradiances for each pixel can be formulated in terms of Eq. (8).

$$E^N_{cell_{i,j}} = \begin{cases} \int_{sunrise}^{sunset} A_{cell}\left(I_b(t) + I_d(t)\right)\mathrm{d}t & \text{if } 250 \le V_{pixel} \le 255 \\ \int_{sunrise}^{sunset} A_{cell} I_d(t)\,\mathrm{d}t & \text{if } 0 \le V_{pixel} < 250 \end{cases} \tag{8}$$

Fourthly, each pixel value in the roof image should also be read in MATLAB programming in order to identify whether it belongs to the building roof. It is assumed that the pixels are displayed as the colour of the building roof. The algorithm implements solar radiation estimation for building roofs by taking into account all pixels from the shadow maps whose positions on the shadow maps have the same position in the building roof image.

The fifth step is to calculate the total solar radiation yield over a building roof for a period by considering multiple instantaneous solar irradiances using a specific time interval. Then solar radiation maps are generated to demonstrate the solar energy potentials of specific regions and provide information for site selection. Specifically, within a given region Ω the solar radiation yield E from the N_1th to N_2th days during a year can be formulated as Eq. (9).

$$E = \sum_{i=1}^{I}\sum_{j=1}^{J} E_{cell_{i,j}} = \sum_{i=1}^{I}\sum_{j=1}^{J}\left(\sum_{N=N_1}^{N_2} E^N_{cell_{i,j}}\right) \quad \left(i \text{ and } j \in \Omega\right) \tag{9}$$

After calculating the solar radiation yield, the radiation distribution within Ω can be mapped as a colour or greyscale image using

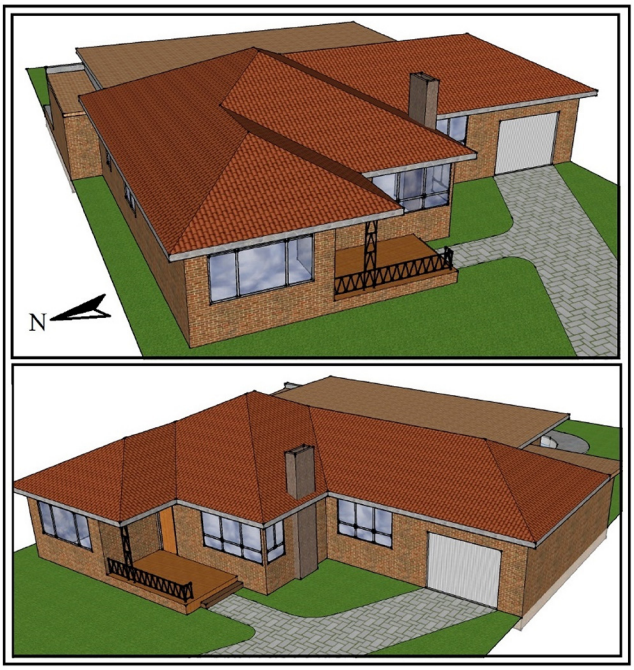

Fig. 3. A pitched-roof building model.

a linear interpolation method. For example, a greyscale solar radiation map can be created on the basis of new pixel values V'_{pixel} which can be formulated as Eq. (10).

$$V'_{pixel} = 255 \times \left(E_{cell_{i,j}} - E_{cell,\ \min}\right) / \left(E_{cell,\ \max} - E_{cell,\ \min}\right) \left(i \text{ and } j \in \Omega\right) \quad (10)$$

$E_{cell,\ \max}$ and $E_{cell,\ \min}$ are set as the maximum and minimum cell solar radiation yields within Ω, respectively.

3. Case study

For the preliminary application of the method proposed in the previous section, an existing residential building, a traditional pitched-roof house in Australia, is chosen as a case study to measure solar energy potential over its roofs. After modification, a corresponding building model is constructed in SketchUp as shown in Fig. 3.

This building is situated in the city of Greater Geelong (Victoria, Australia), so the model is geo-located by entering the longitude and latitude of Geelong (38.1499°S, 144.3617°E) in SkethUp. More complex topographic features can also be constructed in the platform to influence shadow situations. At this stage, the research only considers a self-shadowing situation in the built environment for estimating the maximum solar radiation potential. This building has a gross floor area of approximately 400 m^2. As labelled in the upper picture of Fig. 4, there are nine roofs on this residential building, excluding Roof J, which has a low load-bearing capability. Roofs A–I have surface areas of 40.58 m^2, 10.74 m^2, 8.60 m^2, 18.35 m^2, 17.08 m^2, 32.01 m^2, 14.34 m^2, 48.91 m^2 and 89.79 m^2. Roofs A–H are pitch-based roofs with the same pitch angle of 26°. Roof A is north facing (the Sun moves through the northern sky at noon in the southern hemisphere). A chimney sits on Roof E. Roof I, which was designed as a flat roof by the architects, has a slight pitch of a few degrees.

Solar energy can be used for reducing a household's energy consumption. In addition, a feed-in tariff is available to households that have a solar energy system of less than 100 kW of generating capacity in Victoria, which means that these households can obtain financial returns for feeding their excess electricity back into the grid. The current Victorian feed-in tariff commenced on

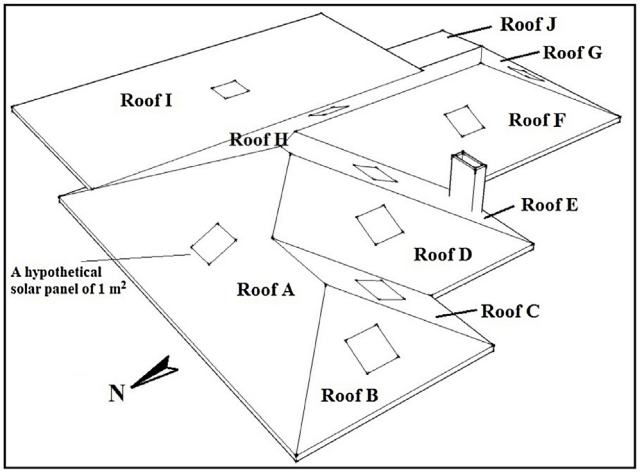

Fig. 4. The house roofs with labels.

1 January 2013 and the minimum feed-in tariff rate of 5 cents per kWh applies from 1 January 2016 [26]. For Australian residential buildings, accurate measurement of solar energy potential is also essential for investigating how specific solar energy devices could contribute to the various energy objectives of cities, businesses and households in social, economic and ecological aspects. In particular, household investors may wish to consider the potential savings on electricity bills and financial returns in solar energy on the basis of accurate assessment and prediction. Therefore, this research chooses a typical Australian house with pitched roofs as a case study to demonstrate the proposed methodology.

4. Estimation of solar radiation

High-accuracy measurement is a key step in accurately evaluating the topographical features of solar radiation over roofs. In this section, high-resolution distribution of solar radiation over roofs is mapped so as to accurately identify roof areas with high radiation intensities and to outline the installation ranges for various solar devices.

4.1. Application to a specific roof

First, the research considers Roof F. The upper-left picture in Fig. 5 depicts a shadow map at 16:00 on 25 July in which shaded pixels are indicated in black. A shadow of the chimney is being cast on the roof and shadow situations concealed by the chimney can be visualised through special treatments. In this study, a shadow map is produced for each hour between sunrise and sunset so that the daily energy yield for each pixel can be calculated by summing the solar potential values for every hour over the same day. A representative daily energy yield is calculated for each day so that the annual energy yield can be obtained with a one-day time step. The roofprint image, sketched in the upper-right picture of Fig. 5, has the same dimensions of 1280 × 720 pixels and each pixel represents a cell with an actual area of 1.7161E–4 m^2. The daily sunshine percentage η for this case study is obtained using the ratio of mean sunshine duration [27] to the ideal daily daylight duration between sunset and sunrise according to the daylight data in SketchUp.

The lower picture in Fig. 5 shows a high-resolution radiation map with 0.0131 m × 0.0131 m cell size, which means the demonstrated results achieve centimetre-level accuracy. Roof F receives an annual total radiation of 1.15E + 5 MJ. The greyscale is presented in terms of Eq. (10), in which $E_{cell,\ \max}$ and $E_{cell,\ \min}$ adopt annual maximum and minimum radiation yields on the roof, namely

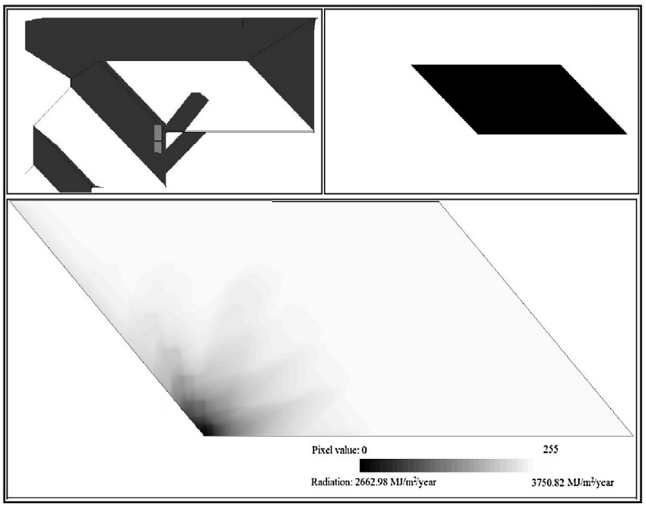

Fig. 5. A shadow map of Roof F at a moment, roofprint and annual radiation map.

3641.69 MJ/m^2/year and 2603.76 MJ/m^2/year respectively. Clearly, most areas are suitable places for installing solar collectors on this roof, except for the bottom-left corner. This is because the shadow of the chimney on Roof E is often projected onto the corner of Roof F in the afternoon.

4.2. Solar radiation maps on the pitched-roof building

The other roofs of the house can also be mapped in greyscale images. In order to differentiate the levels of solar radiation over all the roofs, this research has come up with an integrated radiation map by defining uniform $E_{cell,\ max}$ and $E_{cell,\ min}$. Based on the SketchUp building model, Fig. 6 shows a coloured 3D solar radiation map from different views. The total annual solar radiation over all roofs is estimated at 1.036E + 6 MJ. The average radiation can reach 33695.97 MJ/m^2/year. The maximum and minimum annual radiation yields are 4409.58 MJ/m^2/year and 327.30 MJ/m^2/year respectively. Such a large range in radiation yield is not easy to visualise through a continuous spectrum. Therefore, 4409.58 MJ/m^2/year is defined as the colour maroon, but 2040 MJ/m^2/year and lower values are set as blue.

Table 1 lists the radiation-related indices of the nine roofs. As expected, the north-facing Roof A is receiving the most solar radiation per unit area of the nine roofs. The solar collectors installed on Roof A can obtain 4404.87 MJ/m^2/year and placing these devices in different areas of this roof has little effect on the converted energy yields as there is no great difference between the maximum and minimum radiation values. Furthermore, Roof A has a relatively large area among the roofs. Therefore, this roof is most suited to the installation of solar collectors.

The flat roof with a slight pitch, Roof I, has a solar radiation intensity of around 4000 MJ/m^2/year, shown as an orange-coloured surface. This roof, the largest roof in area, can receive 355,369.39 MJ in annual solar radiation yield. In different seasons, the summer solar radiation yield accounts for 40% of the total annual solar radiation yield, spring for 30%, autumn for 20% and winter for 10%. As a suitable place for installing solar devices, Roof I is second only to Roof A.

In addition, it is observed that the east-facing and west-facing roofs can obtain average annual radiation yields of around 3600 MJ/m^2/year, which is less by around 18% and 9% compared with the radiation yields of the north-facing and flat roofs, respectively. All the west-facing roofs, namely Roofs B, D and F, can achieve the same maximum annual radiation yield, 3641.69 MJ/m^2/year.

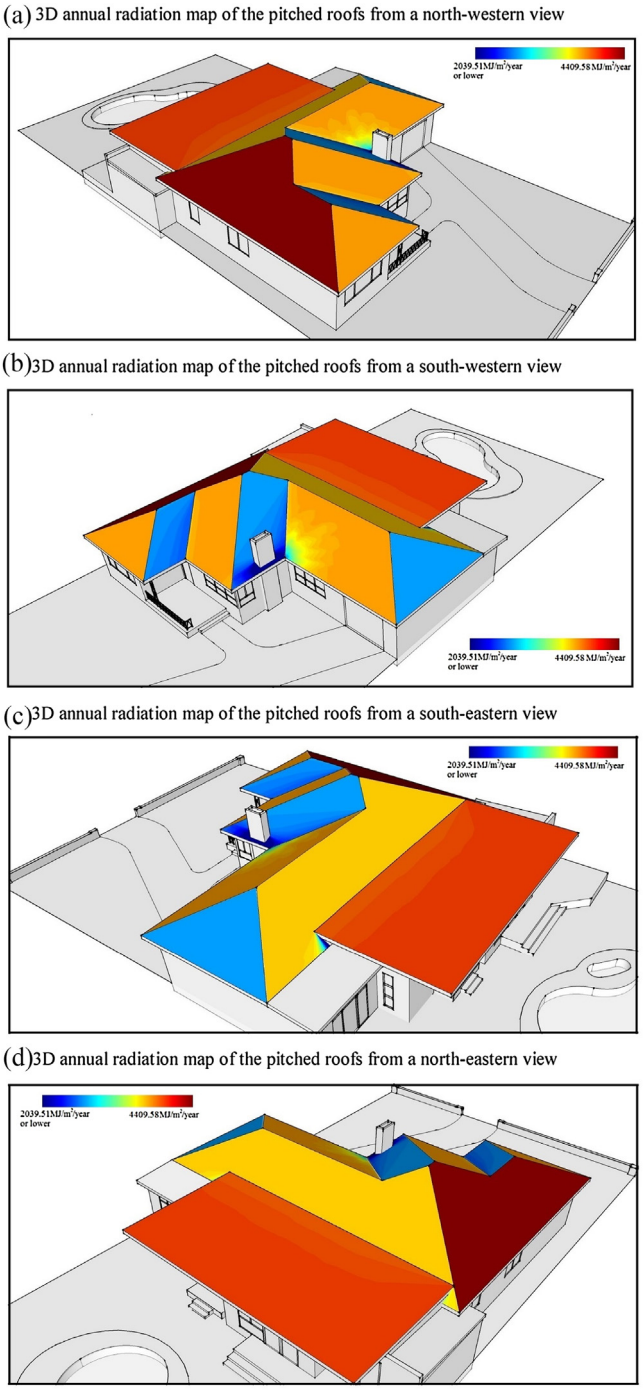

Fig. 6. A 3D annual radiation map on the pitch roofs.

Fig. 6(c) clearly shows that the lowest radiation area of Roof H lies under Roof I and is frequently shaded by this flat roof.

Average annual yields of around 2600 MJ/m^2/year indicate that the least solar radiation strikes the south-facing roofs. These roofs also have relatively small areas. In particular, Roof E can be considered the least suitable place to install solar panels as a chimney sits on this roof. However, this roof is a very interesting case for demonstrating the effects on solar radiation potential of a chimney. Fig. 7 shows the seasonal radiation maps of Roof E. As listed in Table 1, the seasonal solar radiation reaches 14044.64 MJ/m^2 in spring, 21355.06 MJ/m^2 in summer, 6277.83 MJ/m^2 in autumn and 2109.99 MJ/m^2 in winter within the roof area of 17.08 m^2. It is estimated that the chimney causes a loss of 4.4% radiation potential in

Table 1
Radiation-related indices for the nine roofs.

Roofs	Area (m^2)	Annual radiation yield (MJ)	Average annual radiation yield (MJ/m^2)	Maximum annual radiation yield (MJ/m^2)	Minimum annual radiation yield (MJ/m^2)	Spring radiation yield (MJ)	Summer radiation yield (MJ)	Autumn radiation yield (MJ)	Winter radiation yield (MJ)
A	40.47	178281.35	4404.87	4409.58	4304.37	51462.42	62439.94	39408.28	24970.71
B	10.74	39030.78	3634.19	3641.69	3634.12	11752.12	15718.50	7496.76	4063.39
C	8.60	22315.60	2594.65	2667.66	2510.91	7167.91	10888.49	3187.62	1071.57
D	18.35	66639.63	3631.45	3641.69	3574.28	20078.68	26848.59	12800.18	6912.19
E	17.08	43787.53	2563.06	2689.39	327.30	14044.64	21355.06	6277.83	2109.99
F	32.01	115180.51	3598.64	3641.69	2603.76	34719.65	46618.11	22022.71	11820.03
G	14.34	38540.12	2688.24	2689.39	2688.23	12324.72	18955.98	5466.51	1792.90
H	48.90	176776.39	3614.71	3622.33	768.72	53350.07	71246.84	33855.55	18323.93
I	89.79	355369.39	3957.91	3976.21	3881.05	106671.00	143771.00	68018.60	36908.78

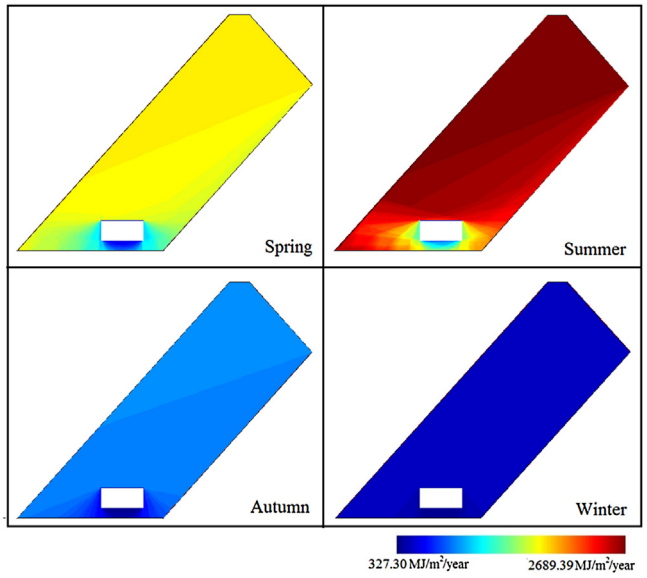

Fig. 7. Seasonal radiation maps of Roof E.

spring, 5.5% in summer, 3.6% in autumn and 1.2% in winter, compared with the corresponding radiation yields without the effects of the chimney. In summer, the roof experiences longer sunshine duration due to greater solar altitude angles and the chimney's shadow projected on Roof E rotates anticlockwise from a 10-o'clock direction to a 2-o'clock direction over a whole summer's day. However, the shadow only rotates anticlockwise between 7-o'clock and 5-o'clock directions over a winter's day. Therefore, objects such as chimneys erected on roofs may lead to losses of solar energy on insolated roofs, particularly in summer.

5. Identification of temporal and spatial distributions for solar radiation potential over roofs

Installing solar panels in the centre of a roof seems common sense. Therefore, in this research, it is assumed that every square solar panel of 1 m^2 is placed on a site on every roof, where it is roughly located at the geometric centre of each roof, as sketched in Fig. 4. Fig. 8 illustrates the variation in the daily solar energy yields that each panel can receive over the whole year. The graph lines coincide with each other for the daily solar energy of panels installed on east-facing and west-facing roofs. South-facing roofs have an almost identical trend, but they maintain a gap that narrows in summer and widens in winter. This is because the greater altitude of the Sun reduces the shading of south-facing roofs in summer. Clearly, more daily radiation can strike solar panels on Roofs A and I. The daily radiation received by the panel on Roof I is more than 100% of that on Roof A in the summer months of January,

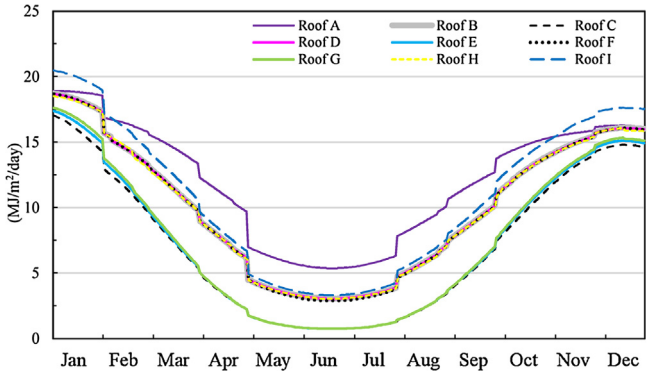

Fig. 8. Changes in daily solar energy received by solar panels over a whole year.

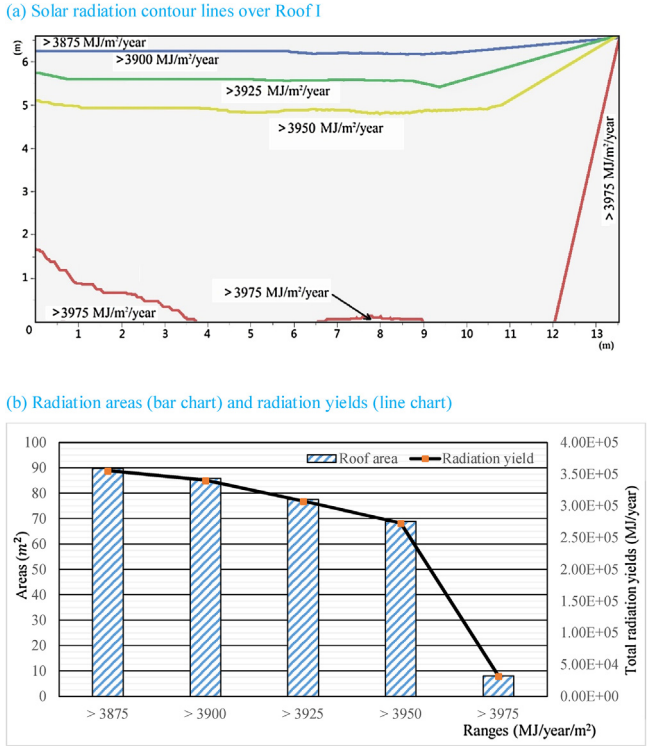

Fig. 9. Topographical features of annual solar radiation over Roof I.

November and December owing to sunlight angles, while it is less than 100% of that on Roof A in other months.

Based on the annual solar radiation yields per unit area over Roof I, Fig. 9 depicts a radiation contour map illustrated with contour lines, which shows the steepness and graduation, and the statistical analysis for different radiation levels. This contour map of annual

radiation illustrates the areas where it is advisable to install common solar water collectors or photovoltaic panels, as these devices are able to receive higher solar radiation yields over the whole year. Therefore, investors may benefit from radiation contour maps.

As shown in Fig. 9a, this contour map uses a 25 MJ contour interval. It can be clearly observed from the radiation contour map that all contour lines cross the upper-right corner, as the dividing line between the shaded and unshaded areas always passes through this corner. A blue line is used to outline the range of 3900 MJ radiation yields, within which the annual solar radiation yields per unit area can reach at least 3900 MJ/m^2/year. There is a gradual decrease in the corresponding areas and radiation yields from 3875 MJ to 3950 MJ regions, as depicted in the bar and line charts. The 3950 MJ and 3975 MJ contour lines illustrate the most suitable places on Roof I for installing solar devices, especially the area between the 3950 MJ and 3975 MJ contour lines, which accounts for 67.67% of the whole roof area and occupies a central region.

Overall, the high-resolution solar radiation maps proposed in this research demonstrate the radiation yields within each unit over pitched roofs with different azimuth angles. These is no significant difference between the radiation yields on each pitched roof except for effects from erected objects. Clearly, north-facing pitched roofs can receive more annual solar radiation (in the southern hemisphere), which means more electricity or hot water can be obtained through solar collectors placed on these roofs. Yet it is possible to achieve more energy conversion in summer when placing collectors on flat roofs, according to the analysis of the daily solar energy received by solar panels over a whole year. Investors may benefit from this analysis when installing solar devices such as solar heating systems with seasonal storage. Energy consumers may also be interested in this type of measurement, as more electricity generated from photovoltaic systems may be consumed by air conditioners in summer. Moreover, the sketched radiation contour lines outline more reasonably and more practically the best areas to install solar devices on roofs.

6. Conclusions

To sum up, estimating solar energy potential over pitched roofs has been selected as a research subject for this paper owing to rapid growth in solar energy applications for residential buildings and in interest in the sustainable development of cities. Most previous research paid extensive attention to LiDAR-based procedures, which are limited to existing buildings and require costly data. In addition, there has been relatively little research on pitched-roof buildings. Thus, taking advantage of building models, this research has constructed a pixel-based method for estimating solar energy potential over pitched roofs so that commercial investors and residents may benefit from more accurate measurement. A typical Australian house with pitched roofs has been chosen as a case study in this research. Based on the platform SketchUp, the shadow situations for this building model have been analysed and a series of greyscale shadow maps produced using the Ruby programming interface. MATLAB programming has then been used to analyse whether every pixel belongs to a shaded area or not, and to estimate the corresponding solar radiation yield for each pixel. Finally, the solar radiation yields have been calculated by considering multiple instantaneous solar irradiances using a specific time interval and visualised by image processing using MATLAB.

The results demonstrate that this method of measurement has the capability to achieve centimetre-level accuracy. The resulting solar radiation maps, including a coloured 3D map and seasonal maps, reveal the nine roofs' radiation distributions including effects from objects erected on the roofs. In addition, the proposed radiation contour map illustrates the optimum ranges for installing solar collectors by identifying the areas of the roofs with high solar potential.

Overall, the proposed method can be applied to assessment measures of solar radiation for commercial energy investors and residents, and the results can contribute to the efficient use of renewable energy sources. The method's algorithm can be easily extended to estimating solar energy potential over the facades of high-rise buildings and specific applications of solar devices could also be taken into account in future research.

References

[1] World Energy Council, 2014 World Energy Issues Monitor, World Energy Council, London, United Kingdom, 2014.
[2] N. Lukač, D. Žlaus, S. Seme, B. Žalik, G. Štumberger, Rating of roofs' surfaces regarding their solar potential and suitability for PV systems, based on LiDAR data, Appl. Energy 102 (2013) 803–812.
[3] X. Fang, D. Li, Solar photovoltaic and thermal technology and applications in China, Renew. Sustain. Energy Rev. 23 (2013) 330–340.
[4] J. Zuo, Z.-Y. Zhao, Green building research—current status and future agenda: a review, Renew. Sustain. Energy Rev. 30 (2014) 271–281.
[5] M. Socorro García-Cascales, M. Teresa Lamata, J. Miguel Sánchez-Lozano, Evaluation of photovoltaic cells in a multi-criteria decision making process, Ann. Oper. Res. 199 (1) (2012) 373–391.
[6] N. Lukač, S. Seme, D. Žlaus, G. Štumberger, B. Žalik, Buildings roofs photovoltaic potential assessment based on LiDAR (Light Detection And Ranging) data, Energy 66 (2014) 598–609.
[7] J. Hofierka, J. Kaňuk, Assessment of photovoltaic potential in urban areas using open-source solar radiation tools, Renew. Energy 34 (10) (2009) 2206–2214.
[8] M. Bizjak, B. Žalik, N. Lukač, Evolutionary-driven search for solar building models using LiDAR data, Energy Build. 92 (2015) 195–203.
[9] J.A. Jakubiec, C.F. Reinhart, A method for predicting city-wide electricity gains from photovoltaic panels based on LiDAR and GIS data combined with hourly Daysim simulations, Sol. Energy 93 (2013) 127–143.
[10] G. Agugiaro, F. Remondino, G. Stevanato, R.D. Filippi, C. Furlanello, Estimation of solar radiation on building roofs in mountainous areas, Int. Arch. Photogramm. Remote Sens. Spat. Inf. Sci. 38 (3/W22) (2011) 155–160.
[11] A. Tereci, D. Schneider, D. Kesten, A. Strzalka, U. Eicker, Energy saving potential and economical analysis of solar systems in the urban quarter Scharnhauser Park, in: Proceedings of the ISES Solar World Congress 2009: Renewable Energy Shaping Our Future, Document Transformation Technologies, Johannesburg, South Africa, 2009.
[12] J. Lee, S. Zlatanova, Solar radiation over the urban texture: LIDAR data and image processing techniques for environmental analysis at city scale, in: J. Lee, S. Zlatanova (Eds.), 3D Geo-Information Sciences, Springer, Berlin, Heidelberg, 2009, pp. 319–340.
[13] P. Redweik, C. Catita, M. Brito, Solar energy potential on roofs and facades in an urban landscape, Sol. Energy 97 (2013) 332–341.
[14] M. Šúri, T.A. Huld, E.D. Dunlop, H.A. Ossenbrink, Potential of solar electricity generation in the European Union member states and candidate countries, Sol. Energy 81 (10) (2007) 1295–1305.
[15] M. Neteler, H. Mitasova, Open Source GIS: A GRASS GIS Approach, Springer, New York, 2008.
[16] J.B. Kodysh, O.A. Omitaomu, B.L. Bhaduri, B.S. Neish, Methodology for estimating solar potential on multiple building rooftops for photovoltaic systems, Sustain. Cities Soc. 8 (2013) 31–41.
[17] N. Lukač, B. Žalik, GPU-based roofs' solar potential estimation using LiDAR data, Comput. Geosci. 52 (2013) 34–41.
[18] J.H. Kämpf, D. Robinson, A hybrid CMA-ES and HDE optimisation algorithm with application to solar energy potential, Appl. Soft Comput. 9 (2) (2009) 738–745.
[19] C. Hachem, A. Athienitis, P. Fazio, Parametric investigation of geometric form effects on solar potential of housing units, Sol. Energy 85 (9) (2011) 1864–1877.
[20] J. Hofierka, M. Zlocha, A new 3-D solar radiation model for 3-D city models, Trans. GIS 16 (5) (2012) 681–690.
[21] J. Liang, J. Gong, W. Li, A.N. Ibrahim, A visualization-oriented 3D method for efficient computation of urban solar radiation based on 3D-2D surface mapping, Int. J. Geogr. Inf. Sci. 28 (4) (2014) 780–798.
[22] Y. Li, D. Ding, C. Liu, C. Wang, A pixel-based approach to estimation of solar energy potential on building roofs, Energy Build. 129 (2016) 563–573.
[23] C. Catita, P. Redweik, J. Pereira, M.C. Brito, Extending solar potential analysis in buildings to vertical facades, Comput. Geosci. 66 (2014) 1–12.
[24] L. Kumar, A.K. Skidmore, E. Knowles, Modelling topographic variation in solar radiation in a GIS environment, Int. J. Geogr. Inf. Sci. 11 (5) (1997) 475–497.
[25] V. Badescu, Modeling Solar Radiation at the Earth's Surface: Recent Advances, Springer Science & Business Media, 2008.
[26] Victorian Government, Victorian Feed-in Tariff, Victorian Government, Melbourne, Australia, 2016.
[27] The Bureau of Meteorology, Average Annual & Monthly Sunshine Duration, The Bureau of Meteorology, Canberra, Australia, 2016.